

Electronic Supporting Information

Engineering cost-effective N-rich metal-organic frameworks (MOFs) for highly efficient CO₂ capture and its catalytic conversion to cyclic carbonates: A step towards sustainable carbon utilization

Mohd Zeeshan^a, Mohammad Yasir Khan^a, M. Shahid*^a, Saiqa Ikram*^b, Musheer Ahmad^c

^a*Functional Inorganic Materials Lab (FIML), Department of Chemistry, Aligarh Muslim University, Aligarh 202002, India.*

^b*Department of Chemistry, Faculty of Sciences, Jamia Millia Islamia (Central University), New Delhi 110025, India*

^c*Department of Applied Chemistry, ZHCET, Aligarh Muslim University, Aligarh 202002, India.*

*Corresponding Authors; E-mail:shahid81chem@gmail.com (M. Shahid), sikram@jmi.ac.in (Saiqa Ikram)

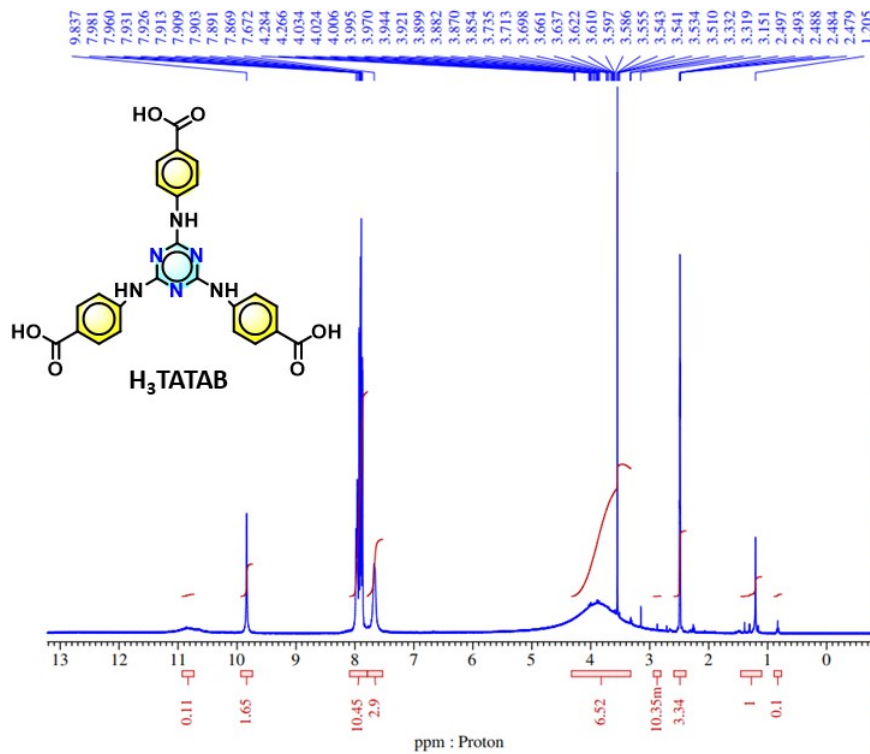


Fig. S1. ^1H NMR spectra of H_3TATAB organic linker (600 MHz, $\text{d}_6\text{-DMSO}$): δ = 7.73 (d, 6H), 8.03 (d, 6H), 8.91 (s, 3H), 12.71 (s, br, 3H)).

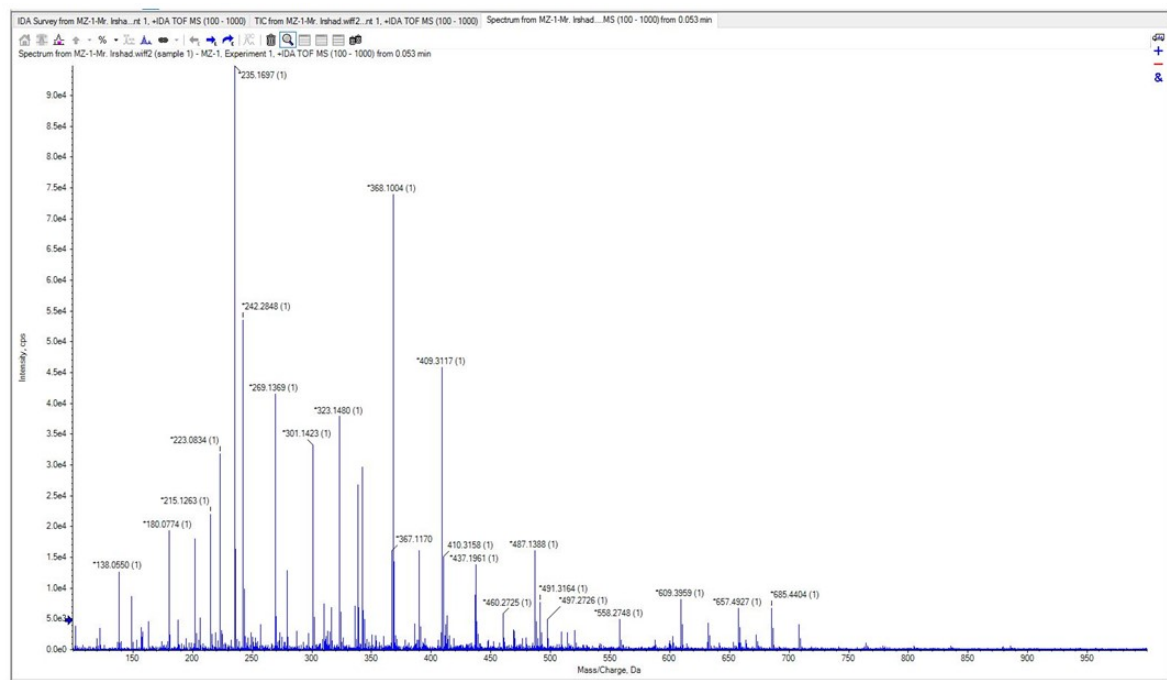


Fig. S2. High resolution mass spectra (HRMS) of H_3TATAB in methanol (m/z = 487.138).

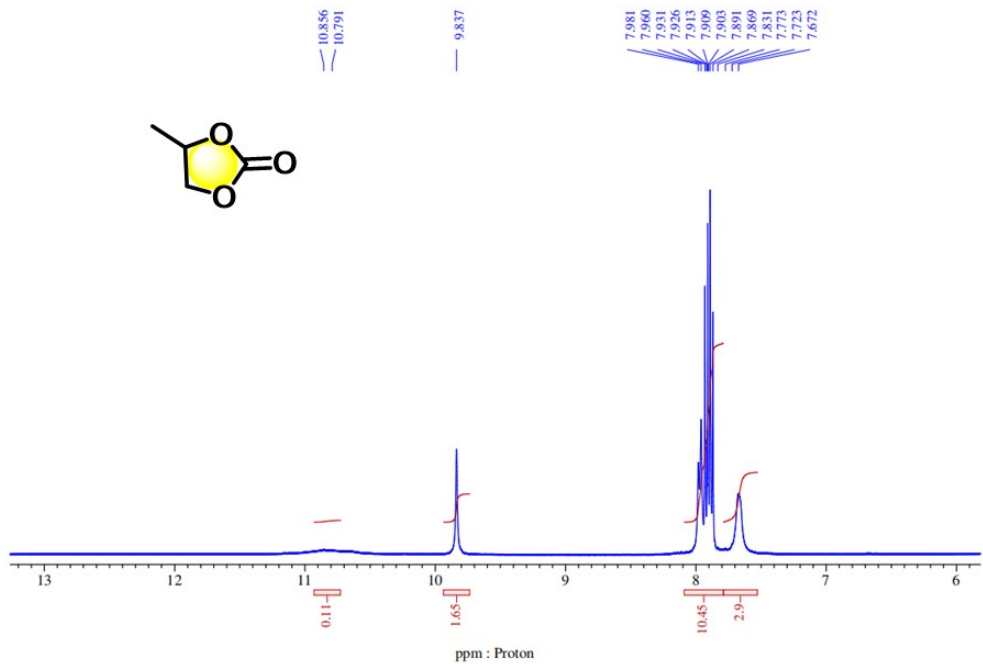


Fig. S3. ¹H NMR spectra of cyclic carbonate **1**.

(¹H NMR (600 MHz, DMSO-d₆) δ 4.88 – 4.80 (m, 1H), 4.55 (t, *J* = 8.0 Hz, 1H), 4.06 (dd, *J* = 8.3, 7.3 Hz, 1H), 1.40 (d, *J* = 6.3 Hz, 3H)).

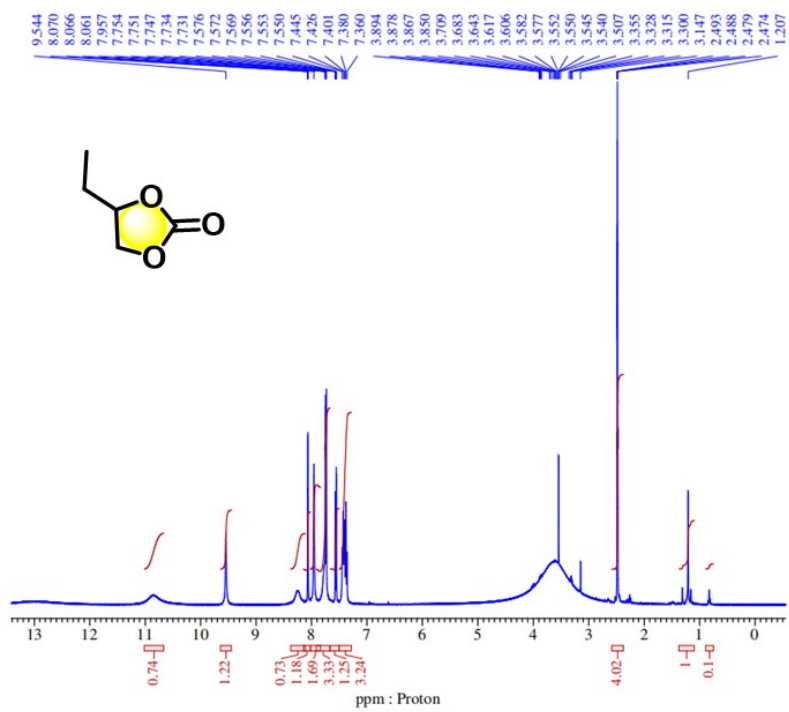


Fig. S4. ¹H NMR spectra of cyclic carbonate **2**.

(¹H NMR (600 MHz, DMSO-d₆) δ 4.68–4.62 (m, 1H), 4.52 (t, *J* = 8.2 Hz, 1H), 4.09–4.05 (m, 1H), 1.84 – 1.68 (m, 2H), 1.01 (t, *J* = 7.5 Hz, 3H)).

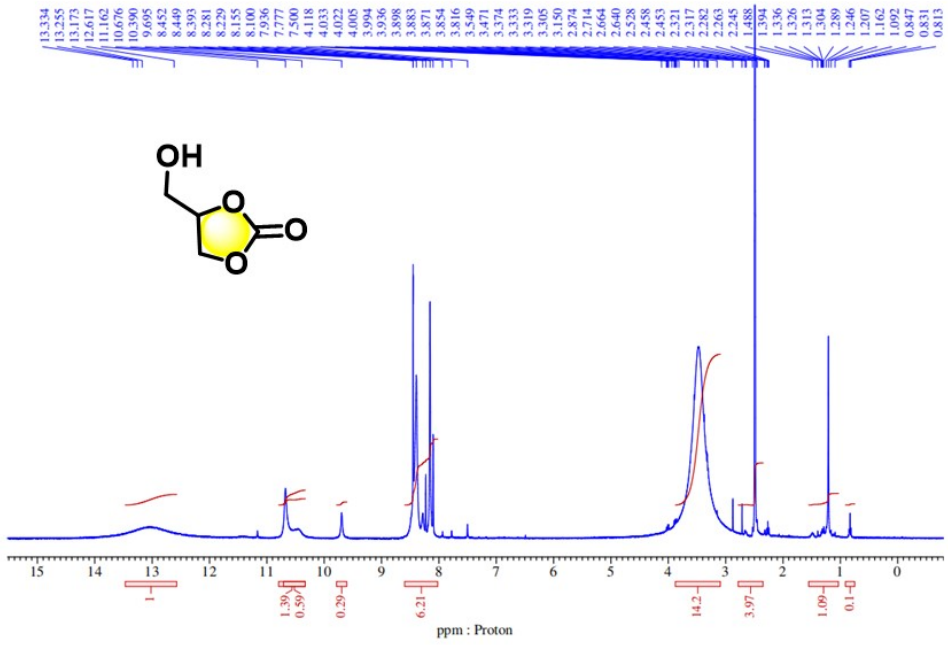


Fig. S5. ^1H NMR spectra of cyclic carbonate 3.

¹H NMR (600 MHz, DMSO-d₆) δ 4.82 (ddd, *J* = 11.6, 6.5, 3.2 Hz, 1H), 4.52 (t, *J* = 8.4 Hz, 1H), 4.45 (dd, *J* = 8.3, 6.6 Hz, 1H), 4.02 (ddd, *J* = 12.9, 5.6, 3.0 Hz, 1H), 3.70 (ddd, *J* = 12.9, 7.0, 3.4 Hz, 1H), 2.83 (t, *J* = 5.9 Hz, 1H)).

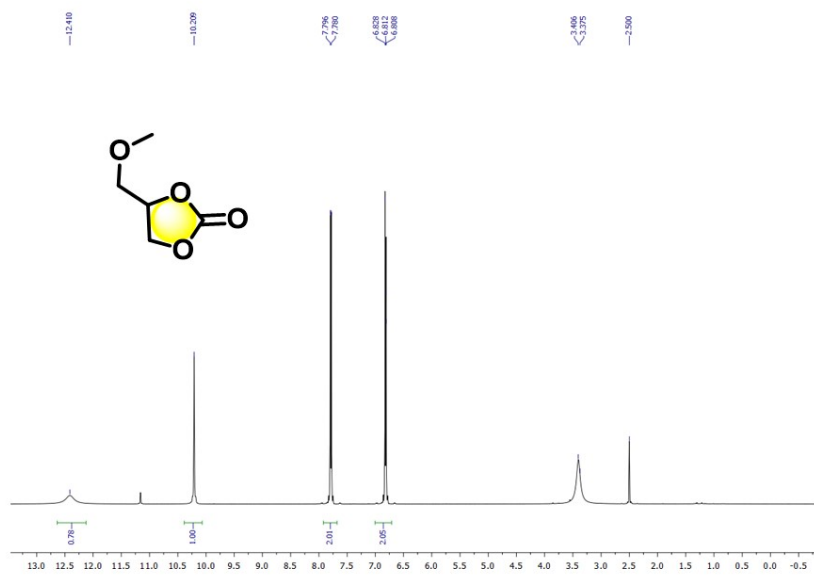


Fig. S6. ^1H NMR spectra of cyclic carbonate 4.

¹H NMR (600 MHz, DMSO-d₆) δ 4.82 – 4.75 (m, 1H), 4.49 (t, *J* = 8.4 Hz, 1H), 4.37 (dd, *J* = 8.4, 6.1 Hz, 1H), 3.64 (dd, *J* = 11.0, 3.8 Hz, 1H), 3.55 (dd, *J* = 11.0, 3.8 Hz, 1H), 3.40 (s, 3H)).

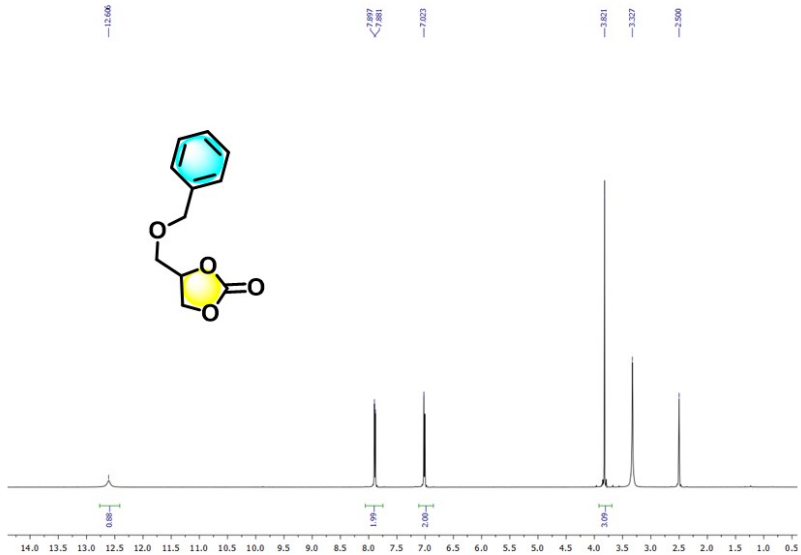


Fig. S7. ^1H NMR spectra of cyclic carbonate **5**.

(^1H NMR (600 MHz, DMSO-d₆) δ 7.36–7.32 (m, 2H), 7.30 – 7.27 (m, 3H), 4.82 – 4.73 (m, 1H), 4.55 (dd, J = 30.3, 12.0 Hz, 2H), 4.45 (t, J = 8.4 Hz, 1H), 4.35 (dd, J = 8.4, 6.0 Hz, 1H), 3.78 (dd, J = 11.0, 3.9 Hz, 1H), 3.62 (dd, J = 11.0, 3.7 Hz, 1H)).

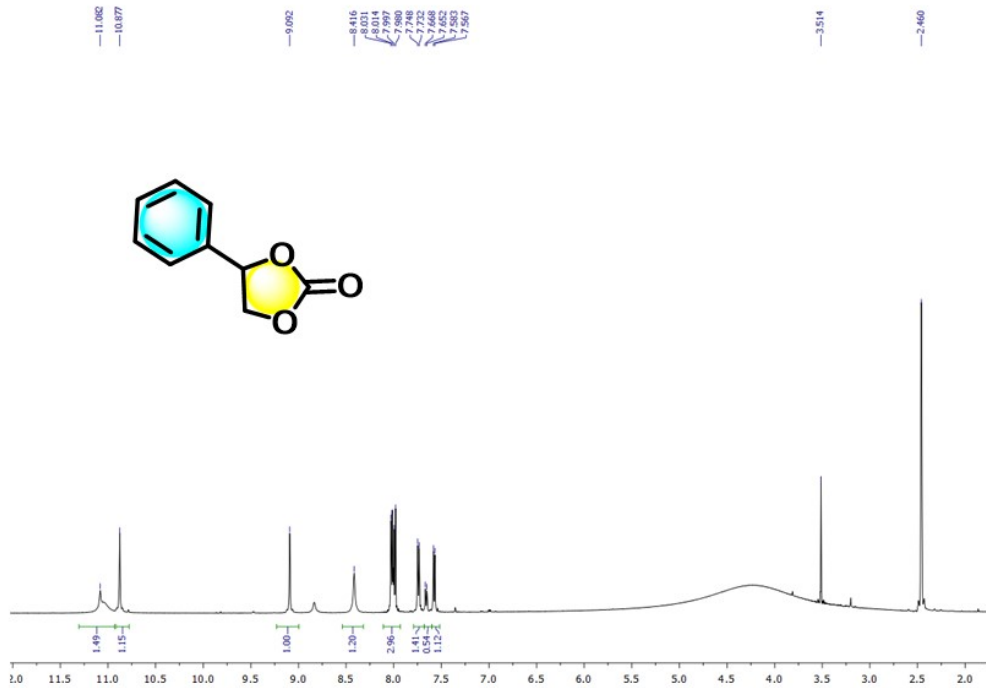


Fig. S8. ^1H NMR spectra of cyclic carbonate **6**.

(^1H NMR (600 MHz, DMSO-d₆) δ 7.48–7.38 (m, 3H), 7.39–7.37 (dd, J = 7.5, 1.6 Hz, 2H), 5.64 (t, J = 8.2 Hz, 1H), 4.82 (t, J = 8.2 Hz, 1H), 4.38–4.34 (m, 1H)).

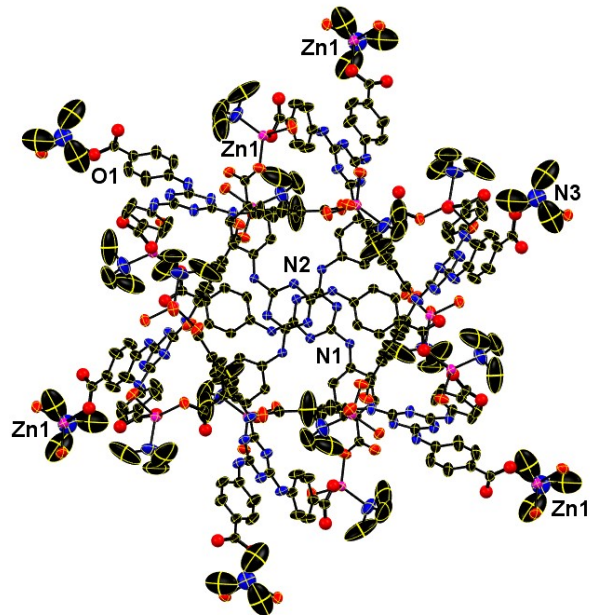


Fig. S9. ORTEP representation of the monomeric unit of **ZS-2** MOF displayed with 50% probability. Atom colours: Zn, magenta polyhedral; N, blue; C and O atoms, black and red spheres, respectively; All hydrogen atoms are omitted for clarity.

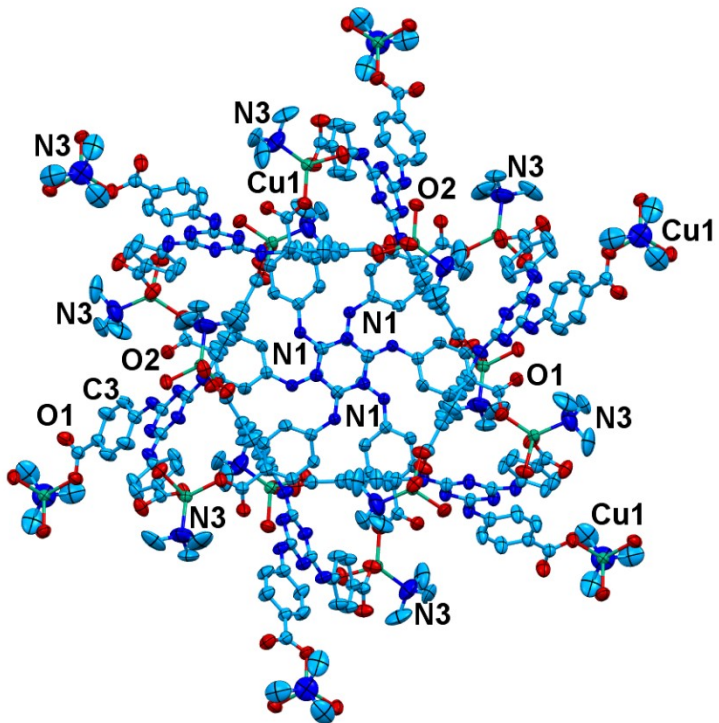


Fig. S10. ORTEP representation of the monomeric unit of **ZS-3** displayed with 50% probability. Atom colours: Cu, green; N, dark blue; C and O atoms, light blue and red spheres, respectively; All hydrogen atoms are omitted for clarity.

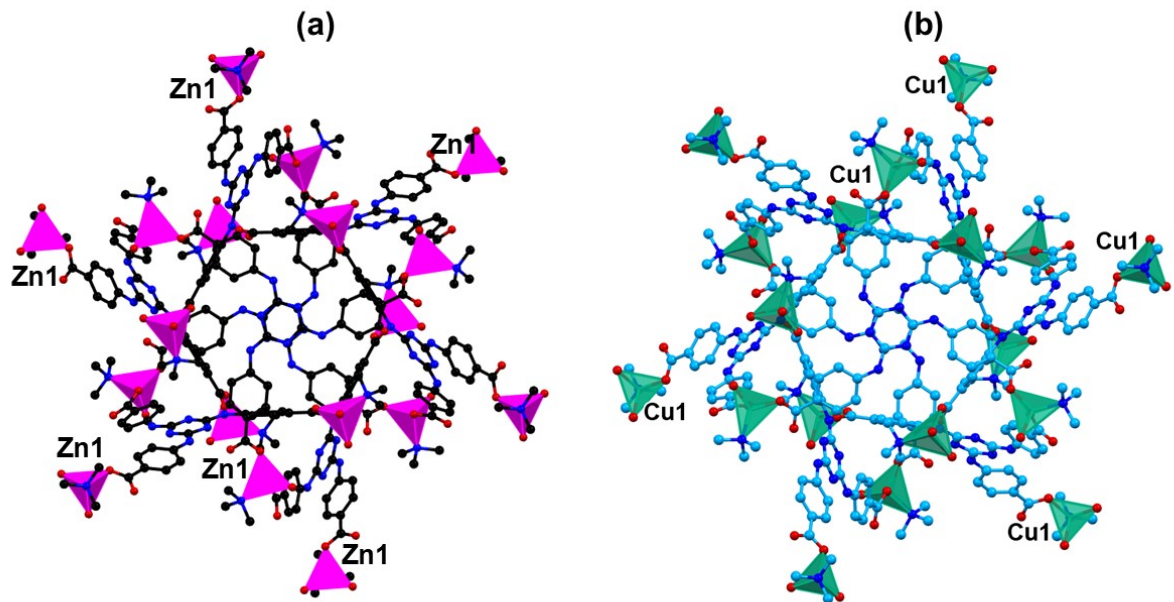


Fig. S11. Polyhedral view along b axis for **ZS-2** (a) and **ZS-3** (b).

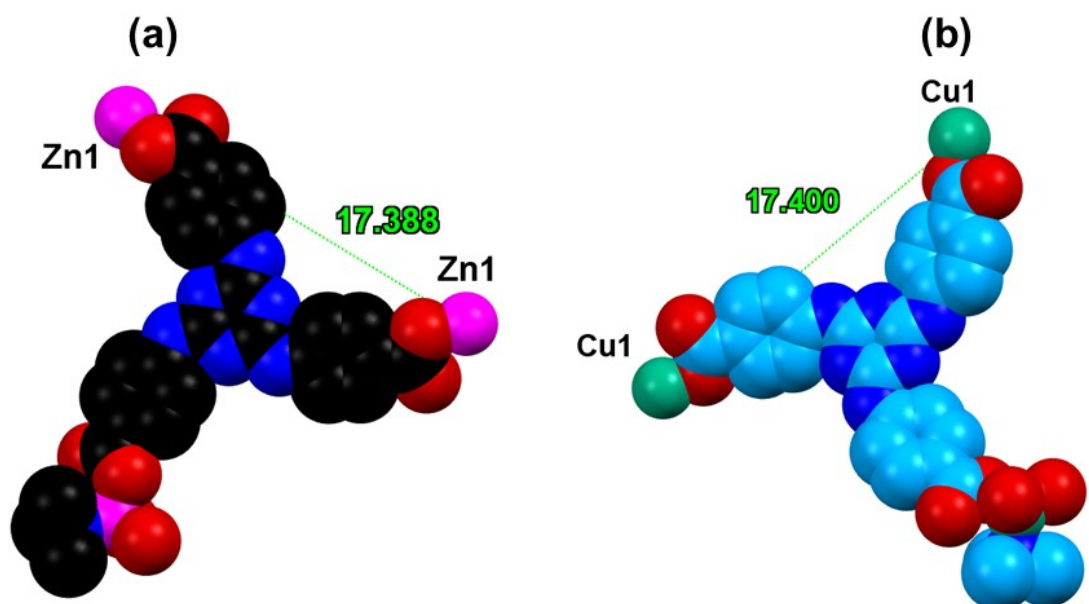


Fig. S12. Space-filling models of Zn- and Cu-based MOFs, showing similar geometric arrangements with nearly identical metal-to-metal distances for **ZS-2** (a) and **ZS-3** (b).

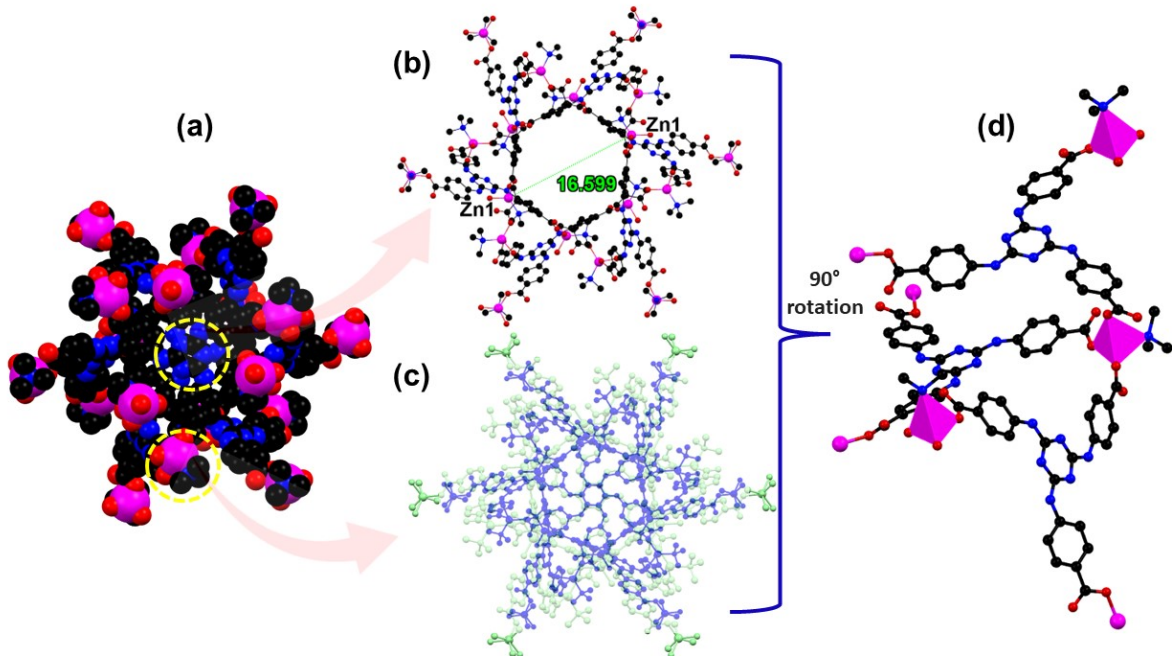


Fig. S13. Space filled model of 3D framework along c axis (a); Crystal structure with bond lengths in angstroms (b); Twofold interpenetrated structure of ZS-2 (c); and Polyhedral structure with extended 3D network after 90° rotation (d). Atom colours: Zn, magenta polyhedral; N, blue; C and O atoms, black and red spheres, respectively; All hydrogen atoms are omitted for clarity.

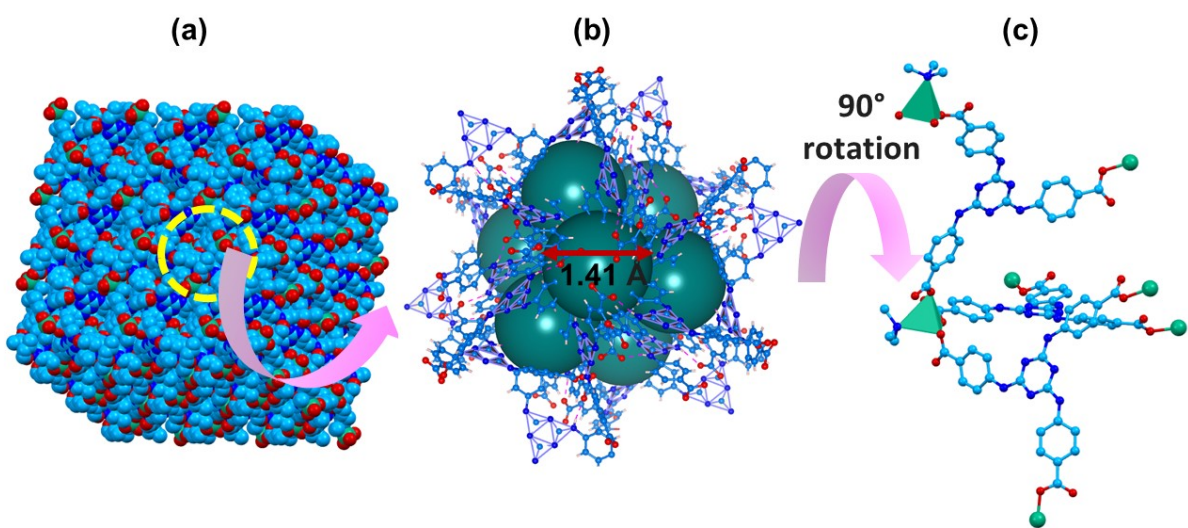


Fig. S14. Space filled model of ZS-3 (a); pore structure with a pore-limiting diameter of 1.41 Å (b); and coordination environment of the metal centers (c).

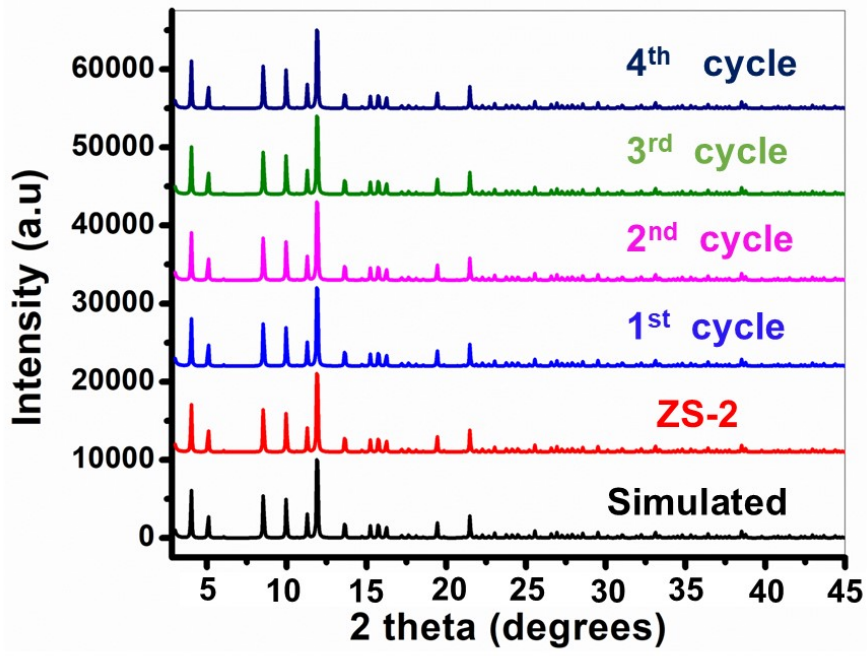


Fig. S15. PXRD plots showing recyclability of ZS-2 up to four consecutive cycles.

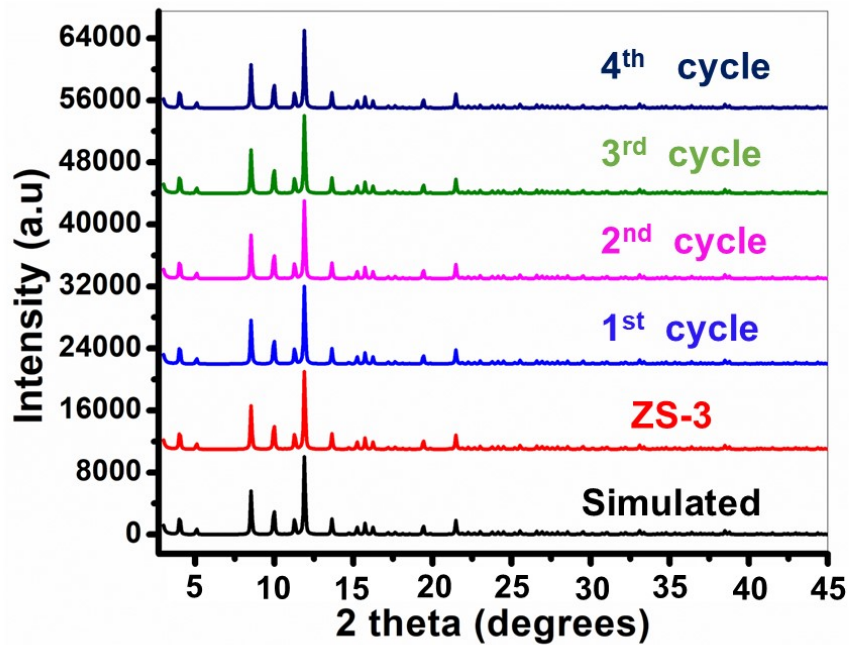


Fig. S16. PXRD plots showing recyclability of ZS-3 up to four consecutive cycles.

Table S1. Crystal data and structure refinement parameters for **ZS-2** and **ZS-3**.

Identification code	ZS-2	ZS-3
CCDC	2431427	2434656
Empirical formula	C ₂₇ H ₂₄ N ₇ O ₆ Zn	C ₅₁ H ₃₉ Cu ₂ N ₁₄ O ₁₂
Formula weight	607.94	1167.10
Temperature/K	293(2)	293(2)
Crystal system	cubic	cubic
Space group	<i>Pa</i> -3	<i>Pa</i> -3
a/Å	19.60237(11)	19.60940(10)
b/Å	19.60237(11)	19.60940(10)
c/Å	19.60237(11)	19.60940(10)
α/°	90	90
β/°	90	90
γ/°	90	90
Volume/Å ³	7532.27(7)	7540.37(7)
Z	7.99992	3.99984
ρcalcg/cm ³	1.0721	1.0280
μ/mm ⁻¹	1.250	1.147
F(000)	2499.4	2379.9
Crystal size/mm ³	0.37 × 0.19 × 0.14	0.34 × 0.22 × 0.16
Radiation	Cu Kα ($\lambda = 1.54184$)	Cu Kα ($\lambda = 1.54184$)
2Θ range for data collection/°	7.82 to 136.3	7.8 to 136.2
Index ranges	-23 ≤ h ≤ 16, -21 ≤ k ≤ 22, -23 ≤ l ≤ 20	-22 ≤ h ≤ 23, -23 ≤ k ≤ 22, -9 ≤ l ≤ 22
Reflections collected	14271	12659
Independent reflections	2289 [R _{int} = 0.0169, R _{sigma} = 0.0101]	2274 [R _{int} = 0.0200, R _{sigma} = 0.0146]
Data/restraints/parameters	2289/0/126	2274/0/126
Goodness-of-fit on F ²	1.026	1.030
Final R indexes [I>=2σ (I)]	R ₁ = 0.0493, wR ₂ = 0.1574	R ₁ = 0.0560, wR ₂ = 0.1680
Final R indexes [all data]	R ₁ = 0.0515, wR ₂ = 0.1596	R ₁ = 0.0580, wR ₂ = 0.1699
Largest diff. peak/hole / e Å ⁻³	0.50/-0.57	1.91/-0.26

Table S2. Fractional Atomic Coordinates ($\times 10^4$) and Equivalent Isotropic Displacement Parameters ($\text{\AA}^2 \times 10^3$) for **ZS-2**. U_{eq} is defined as 1/3 of the trace of the orthogonalised U_{IJ} tensor.

Atom	x	y	z	U(eq)
Zn1	6018.99(14)	1018.99(14)	3981.01(14)	38.2(3)
O1	5476.7(8)	1507.7(10)	4651.1(9)	55.1(5)
O2	6388.0(9)	1912.6(11)	5176.2(10)	59.3(5)
N2	3205.9(10)	1741.4(10)	7370.5(10)	44.6(5)
N1	4060.0(9)	2567.8(11)	7372.8(11)	47.8(5)
C1	5770.1(11)	1794.4(12)	5155.6(12)	41.8(5)
C8	3482.5(11)	2291.0(12)	7648.8(11)	40.3(5)
C5	4451.4(12)	2344.9(12)	6816.0(12)	43.4(5)
C2	5315.6(12)	1988.6(12)	5734.4(12)	42.8(5)
C6	5103.5(13)	2616.6(14)	6762.9(14)	56.9(7)
C7	5525.7(13)	2440.1(15)	6232.0(14)	58.5(7)
C3	4668.4(14)	1722.8(15)	5791.3(14)	61.4(8)
C4	4242.1(14)	1891.4(17)	6321.2(15)	66.5(8)
N3	6614.9(14)	1614.9(14)	3385.1(14)	100.5(19)
C9	6628(4)	1362(6)	2661(3)	245(5)

Table S3. Anisotropic Displacement Parameters ($\text{\AA}^2 \times 10^3$) for **ZS-2**. The Anisotropic displacement factor exponent takes the form: $-2\pi^2[h^2a^*{}^2U_{11}+2hka^*b^*U_{12}+\dots]$.

Atom	U_{11}	U_{22}	U_{33}	U_{12}	U_{13}	U_{23}
Zn1	38.2(3)	38.2(3)	38.2(3)	-0.73(11)	0.73(11)	0.73(11)
O1	41.5(9)	73.1(12)	50.9(10)	3.8(8)	1.1(7)	-21.1(9)
O2	41.0(9)	76.4(12)	60.5(11)	-12.1(9)	8.3(8)	-20.5(9)
N2	43.8(10)	43.6(10)	46.4(11)	-9.2(8)	10.3(8)	-8.4(8)
N1	44.2(10)	48.9(11)	50.2(12)	-15.3(9)	14.1(9)	-15.2(9)
C1	40.8(12)	41.1(11)	43.4(12)	-2.8(9)	0.4(10)	-6.7(9)
C8	39.2(11)	41.2(11)	40.4(11)	-5.0(9)	5.1(9)	-4.3(9)
C5	42.9(12)	45.4(12)	42.0(11)	-8.0(10)	5.5(9)	-5.6(10)
C2	39.8(11)	45.8(12)	42.9(12)	-3.9(9)	3.8(9)	-5.5(10)
C6	46.5(13)	66.2(16)	58.1(15)	-17.7(12)	10.5(11)	-28.2(13)
C7	40.1(12)	74.2(18)	61.2(15)	-18.6(12)	10.4(12)	-25.2(14)
C3	55.3(15)	75.6(18)	53.2(15)	-26.9(14)	11.4(12)	-26.2(14)
C4	50.2(15)	89(2)	60.4(16)	-32.2(14)	18.6(13)	-30.5(15)
N3	100.5(19)	100.5(19)	100.5(19)	-30.3(15)	30.3(15)	30.3(15)
C9	188(8)	391(15)	155(6)	50(9)	75(6)	143(8)

Table S4. Bond Lengths for **ZS-2**.

Atom	Atom	Length/Å		Atom	Atom	Length/Å
Zn1	O1 ¹	1.9423(17)		C1	C2	1.492(3)
Zn1	O1 ²	1.9423(17)		C5	C6	1.389(3)
Zn1	O1	1.9423(17)		C5	C4	1.378(3)
Zn1	N3	2.023(5)		C2	C7	1.380(3)
O1	C1	1.275(3)		C2	C3	1.376(3)
O2	C1	1.234(3)		C6	C7	1.374(4)
N2	C8 ³	1.351(3)		C3	C4	1.373(4)
N2	C8	1.324(3)		N3	C9	1.504(8)
N1	C8	1.367(3)		N3	C9 ¹	1.504(8)
N1	C5	1.404(3)		N3	C9 ²	1.504(8)

Table S5. Bond Angles for **ZS-2**.

Atom	Atom	Atom	Angle/°		Atom	Atom	Atom	Angle/°
O1	Zn1	O1 ¹	103.49(6)		C4	C5	C6	117.9(2)
O1 ²	Zn1	O1 ¹	103.49(7)		C7	C2	C1	121.5(2)
O1 ²	Zn1	O1	103.49(6)		C3	C2	C1	121.0(2)
N3	Zn1	O1 ¹	114.94(6)		C3	C2	C7	117.4(2)
N3	Zn1	O1	114.94(6)		C7	C6	C5	121.0(2)
N3	Zn1	O1 ²	114.94(6)		C6	C7	C2	121.1(2)
C1	O1	Zn1 ²	119.69(15)		C4	C3	C2	122.1(2)
C5	N1	C8	129.54(19)		C3	C4	C5	120.4(2)
O2	C1	O1	123.4(2)		C9	N3	Zn1	111.4(4)
C2	C1	O1	115.67(19)		C9 ²	N3	Zn1	111.4(4)
C2	C1	O2	120.9(2)		C9 ¹	N3	Zn1	111.4(4)
N1	C8	N2 ³	113.20(18)		C9 ¹	N3	C9	107.5(4)
N1	C8	N2	119.95(19)		C9 ¹	N3	C9 ²	107.5(4)
C6	C5	N1	116.2(2)		C9 ²	N3	C9	107.5(4)
C4	C5	N1	125.8(2)					

Table S6. Hydrogen Atom Coordinates ($\text{\AA} \times 10^4$) and Isotropic Displacement Parameters ($\text{\AA}^2 \times 10^3$) for **ZS-2**.

Atom	x	y	z	U(eq)
H3	4514.7(14)	1419.3(15)	5460.6(14)	73.6(9)
H4	3809.4(14)	1698.4(17)	6346.2(15)	79.8(10)
H6	5256.7(13)	2922.6(14)	7091.6(14)	68.3(9)
H7	5960.5(13)	2628.2(15)	6207.6(14)	70.2(9)
H1	4205.0(9)	2932.3(11)	7569.3(11)	57.4(6)
H9a	6730(50)	883(12)	2657(4)	367(7)
H9b	6190(17)	1440(50)	2454(16)	367(7)
H9c	6970(30)	1600(40)	2410(13)	367(7)

Table S7. Fractional Atomic Coordinates ($\times 10^4$) and Equivalent Isotropic Displacement Parameters ($\text{\AA}^2 \times 10^3$) for **ZS-3**. U_{eq} is defined as 1/3 of the trace of the orthogonalised U_{IJ} tensor.

Atom	x	y	z	U(eq)
Cu1	-1020.42(18)	6020.42(18)	3979.58(18)	40.4(3)
O2	-469.0(10)	6506.7(12)	4648.7(11)	62.7(6)
O1	-1378.7(10)	6909.8(13)	5168.7(12)	67.6(6)
N2	1790.1(12)	6734.1(12)	7375.1(11)	49.8(6)
N1	935.3(12)	7558.4(13)	7379.9(12)	53.3(6)
C8	1512.4(13)	7289.0(13)	7650.4(13)	44.6(6)
C5	546.1(14)	7340.3(14)	6818.3(14)	48.2(6)
C1	-762.1(13)	6792.3(14)	5150.1(14)	47.7(6)
C2	-306.9(13)	6988.5(14)	5730.7(14)	48.7(6)
C4	-117.2(15)	7592.4(18)	6773.3(17)	64.2(9)
C7	348.4(15)	6740.1(17)	5777.4(16)	61.4(8)
C3	-530.8(16)	7420.3(18)	6240.5(17)	64.0(9)
C6	770.5(16)	6901.1(18)	6316.7(17)	64.9(9)
N3	-1616.9(18)	6616.9(18)	3383.1(18)	115(2)
C19	-1345(7)	7327(5)	3341(6)	123(4)

Table S8. Anisotropic Displacement Parameters ($\text{\AA}^2 \times 10^3$) for **ZS-3**. The Anisotropic displacement factor exponent takes the form: $-2\pi^2[h^2a^*{}^2U_{11}+2hka^*b^*U_{12}+\dots]$.

Atom	U_{11}	U_{22}	U_{33}	U_{12}	U_{13}	U_{23}
Cu1	40.4(3)	40.4(3)	40.4(3)	0.49(14)	-0.49(14)	0.49(14)
O2	50.1(11)	79.3(14)	58.8(12)	-1.4(10)	-2.1(9)	-24.8(11)
O1	47.7(11)	86.3(15)	68.8(13)	14.4(11)	-9.5(10)	-23.8(12)
N2	50.6(12)	49.3(12)	49.6(12)	10.0(10)	-10.4(10)	-8.4(10)
N1	50.7(12)	54.1(13)	55.2(13)	15.2(10)	-14.7(10)	-16.4(11)
C8	43.8(13)	45.2(13)	44.9(13)	4.5(10)	-5.8(11)	-5.4(11)
C5	46.8(14)	49.7(14)	48.2(14)	7.6(11)	-8.4(11)	-6.6(11)
C1	44.0(14)	50.7(14)	48.3(14)	2.5(11)	-1.7(11)	-2.7(11)
C2	44.9(13)	51.5(14)	49.6(14)	5.4(11)	-3.1(11)	-5.9(12)
C4	51.9(16)	78(2)	63.3(18)	21.7(15)	-10.2(14)	-30.9(16)
C7	50.3(16)	77(2)	57.4(16)	19.9(14)	-7.9(13)	-24.7(15)
C3	47.3(15)	78(2)	67.1(18)	19.7(14)	-11.4(14)	-23.8(16)
C6	49.0(16)	85(2)	60.6(17)	26.8(15)	-11.2(14)	-23.2(16)
N3	115(2)	115(2)	115(2)	33(2)	-33(2)	33(2)
C19	164(10)	78(5)	128(8)	53(6)	27(8)	54(6)

Table S9. Bond Lengths for **ZS-3**.

Atom	Atom	Length/Å	Atom	Atom	Length/Å
Cu1	O2 ¹	1.949(2)	C5	C4	1.394(4)
Cu1	O2	1.949(2)	C5	C6	1.380(4)
Cu1	O2 ²	1.949(2)	C1	C2	1.497(4)
Cu1	N3	2.026(6)	C2	C7	1.377(4)
O2	C1	1.269(3)	C2	C3	1.382(4)
O1	C1	1.232(3)	C4	C3	1.365(4)
N2	C8	1.331(3)	C7	C6	1.379(4)
N2	C8 ³	1.351(3)	N3	C19 ²	1.493(11)
N1	C8	1.357(3)	N3	C19	1.493(11)
N1	C5	1.407(3)	N3	C19 ¹	1.493(11)

Table S10. Bond Angles for **ZS-3**.

Atom	Atom	Atom	Angle/°	Atom	Atom	Atom	Angle/°
O2	Cu1	O2 ¹	103.13(11)	C2	C1	O1	121.0(2)
O2 ²	Cu1	O2 ¹	103.13(9)	C7	C2	C1	121.1(2)
O2 ²	Cu1	O2	103.13(11)	C3	C2	C1	121.2(2)
N3	Cu1	O2 ¹	115.24(7)	C3	C2	C7	117.7(3)
N3	Cu1	O2	115.24(7)	C3	C4	C5	121.0(3)
N3	Cu1	O2 ²	115.24(7)	C6	C7	C2	122.0(3)
C1	O2	Cu1 ²	119.09(18)	C4	C3	C2	121.1(3)
C5	N1	C8	129.8(2)	C7	C6	C5	119.9(3)
N1	C8	N2 ³	113.3(2)	C19 ²	N3	Cu1	111.4(5)
N1	C8	N2	120.1(2)	C19	N3	Cu1	111.4(5)
C4	C5	N1	116.6(2)	C19 ¹	N3	Cu1	111.4(5)
C6	C5	N1	125.1(2)	C19 ¹	N3	C19 ²	107.5(6)
C6	C5	C4	118.3(3)	C19 ¹	N3	C19	107.5(7)
O1	C1	O2	123.4(3)	C19	N3	C19 ²	107.5(7)
C2	C1	O2	115.6(2)				

Table S11. Hydrogen Atom Coordinates ($\text{\AA} \times 10^4$) and Isotropic Displacement Parameters ($\text{\AA}^2 \times 10^3$) for **ZS-3**.

Atom	x	y	z	U(eq)
H3	-970.6(16)	7596.6(18)	6220.3(17)	76.8(10)
H4	-280.3(15)	7882.2(18)	7111.5(17)	77.1(10)
H6	1205.5(16)	6713.9(18)	6342.0(17)	77.9(10)
H7	511.3(15)	6455.2(17)	5435.0(16)	73.7(10)
H1	784.6(12)	7917.0(13)	7582.7(12)	64.0(7)
H19a	-1310(50)	7520(20)	3791(8)	185(6)
H19b	-900(20)	7320(7)	3130(50)	185(6)
H19c	-1650(30)	7601(14)	3070(50)	185(6)

Table S12. Atomic Occupancy for **ZS-3**.

Atom	Occupancy	Atom	Occupancy	Atom	Occupancy
C19	0.500000	H19a	0.500000	H19b	0.500000
H19c	0.500000				

Table S13. Solvent masks information for **ZS-3**.

Number	X	Y	Z	Volume	Electron count
1	0.000	0.000	0.000	30.0	0.0
2	0.000	0.000	0.500	677.9	191.3
3	0.000	0.500	0.000	677.9	191.3
4	0.000	0.500	0.500	30.0	0.0
5	0.500	0.000	0.000	677.9	191.3
6	0.500	0.500	0.500	677.9	191.3
7	0.500	0.000	0.500	30.0	0.0
8	0.500	0.500	0.000	30.0	0.0

1. Control experiments for evaluating the role of **ZS-2** and **ZS-3** and co-catalysts

To validate the intrinsic catalytic performance of the synthesized MOFs (**ZS-2** and **ZS-3**), a series of control experiments were carried out using individual components and their combinations under identical reaction conditions. These included the use of $\text{Zn}(\text{NO}_3)_2 \cdot 6\text{H}_2\text{O}$, $\text{Cu}(\text{NO}_3)_2 \cdot 3\text{H}_2\text{O}$, the tritopic H_3TATAB linker, and various tetrabutylammonium halide salts (nBu_4NCl , nBu_4NBr , nBu_4NI). Additionally, physical mixtures of metal salts and the ligand were tested with each co-catalyst. The conversion values for each system were determined by gas chromatography using a flame ionization detector (GC-FID), with biphenyl as the internal standard. Among the co-catalysts, nBu_4NBr exhibited the highest catalytic performance when used with both MOFs, showing significantly higher conversion compared to Cl^- and I^- analogs. In contrast, reactions using only the metal salts, ligand, or their combinations resulted in poor conversion (<30%), and co-catalyst-only systems showed minimal activity (<6%). These results confirm that the well-defined porous framework of the MOFs, in combination with an optimal halide co-catalyst, is essential for efficient CO_2 -epoxide cycloaddition. The findings support the conclusion that the MOFs act as true heterogeneous catalysts, with their structure playing a crucial role in enhancing the reaction outcome.

Table S14. Control experiments to check catalytic activity using various tetrabutylammonium halides with **ZS-2** and **ZS-3** along with metal salts, ligand, and their combinations (Reaction conditions: H₃TATAB (1 mol%), pre-activated MOF catalyst (0.36 mol %), metal salts (0.2 mol%), and co-catalysts like nBu₄NCl, nBu₄NBr, and nBu₄NI (each with 0.045 mmol, 1 mol %)).

Entry	Catalyst used	% Conversion
1.	ZS-2 + nBu ₄ NCl	95.50
2.	ZS-2 + nBu ₄ NBr	96.84
3.	ZS-2 + nBu ₄ NI	96.23
4.	ZS-3 + nBu ₄ NCl	94.56
5.	ZS-3 + nBu ₄ NBr	95.78
6.	ZS-3 + nBu ₄ NI	95.56
7.	Zn(NO ₃) ₂ ·6H ₂ O + nBu ₄ NCl	18.20
8.	Zn(NO ₃) ₂ ·6H ₂ O + nBu ₄ NBr	22.53
9.	Zn(NO ₃) ₂ ·6H ₂ O + nBu ₄ NI	21.67
10.	Cu(NO ₃) ₂ ·3H ₂ O + nBu ₄ NCl	16.60
11.	Cu(NO ₃) ₂ ·3H ₂ O + nBu ₄ NBr	19.80
12.	Cu(NO ₃) ₂ ·3H ₂ O + nBu ₄ NI	18.34
13.	H ₃ TATAB only	2.300
14.	H ₃ TATAB + nBu ₄ NCl	6.145
15.	H ₃ TATAB + nBu ₄ NBr	6.576
16.	H ₃ TATAB + nBu ₄ NI	5.845
17.	Zn(NO ₃) ₂ ·6H ₂ O + H ₃ TATAB + nBu ₄ NCl	26.24
18.	Zn(NO ₃) ₂ ·6H ₂ O + H ₃ TATAB + nBu ₄ NBr	28.42
19.	Zn(NO ₃) ₂ ·6H ₂ O + H ₃ TATAB + nBu ₄ NI	26.76
20.	Cu(NO ₃) ₂ ·3H ₂ O + H ₃ TATAB + nBu ₄ NCl	23.52
21.	Cu(NO ₃) ₂ ·3H ₂ O + H ₃ TATAB + nBu ₄ NBr	27.56
22.	Cu(NO ₃) ₂ ·3H ₂ O + H ₃ TATAB + nBu ₄ NI	26.67
23.	nBu ₄ NCl only	5.243
24.	nBu ₄ NBr only	5.657
25.	nBu ₄ NI only	5.543

2. Leaching test to confirm heterogeneous nature of **ZS-2** and **ZS-3** catalyst

To confirm the heterogeneous nature of the MOF catalyst used in the cycloaddition of CO₂ with various epoxides, a hot filtration test was carried out under optimized reaction conditions. The reaction was conducted using different epoxides in the presence of the MOF catalyst and quaternary ammonium halide co-catalysts (nBu₄NCl, nBu₄NBr, and nBu₄NI) at 80 °C under 2 MPa CO₂ pressure. After 3 hours of reaction, the hot reaction mixture was rapidly filtered to remove the solid MOF catalyst, ensuring no reprecipitation of dissolved

species. The clear filtrate was then returned to the reactor and stirred under identical conditions for an additional 5 hours. GC-FID analysis revealed that the reaction conversion prior to catalyst removal was approximately 58.6%, while the filtrate exhibited negligible additional conversion (< 1.2%) thereafter, confirming the absence of catalytically active species in solution. Furthermore, ICP-OES analysis of the filtrate showed that the metal ion concentrations were below the detectable limit (< 0.5 ppm), supporting minimal leaching during the reaction. These results collectively confirm that the catalytic activity originates solely from the solid MOF, verifying its role as a stable, reusable, and truly heterogeneous catalyst for CO₂ fixation into cyclic carbonates using different epoxides and co-catalysts.

Table S15. ICP-OES analysis confirming negligible leaching from **ZS-2** and **ZS-3**, supporting their heterogeneous catalytic nature.

Sample	ZS-2 (ppm)	ZS-3 (ppm)
Fresh MOF	1.25%	1.18%
MOF after reaction	0.15	0.10
Filtrate after catalyst removal	< 0.5 (not detected)	< 0.5 (not detected)

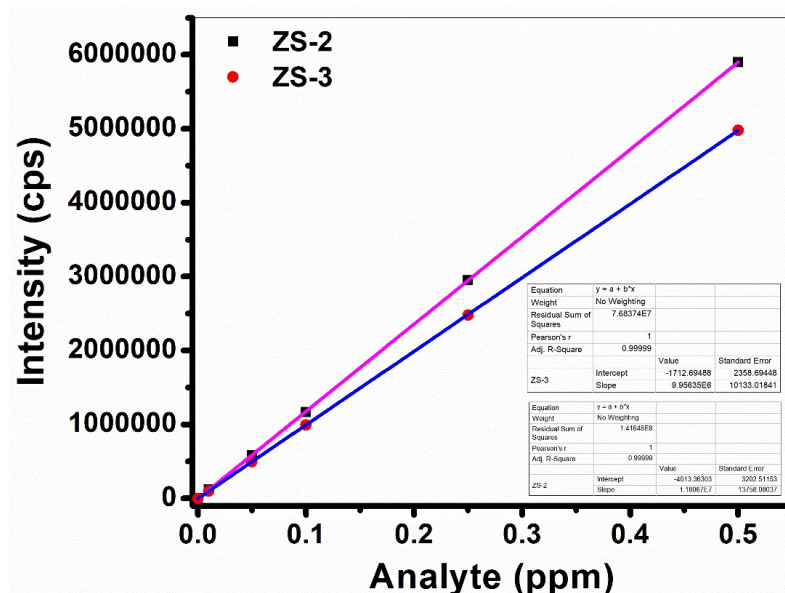


Fig. S17. ICP-OES calibration curves for **ZS-2** and **ZS-3** showing linear response up to 0.5 ppm. Filtrate signals fall below detection limit, confirming negligible metal leaching.

Table S16. Data showing retention times and peak areas of different epoxides including side products and main products analysed by GC-FID.

Entry	Epoxides	Retention time (min)	Peak area (Unreacted epoxide)	Peak area (Cyclic carbonate)	Peak area (Side products)	Peak area (Biphenyl)
1.		4.8	700	2800	900	1000
2.		5.1	650	3000	850	1000
3.		5.4	600	3200	800	1000
4.		5.6	550	3400	750	1000
5.		5.9	500	3600	700	1000
6.		6.2	450	3800	650	1000

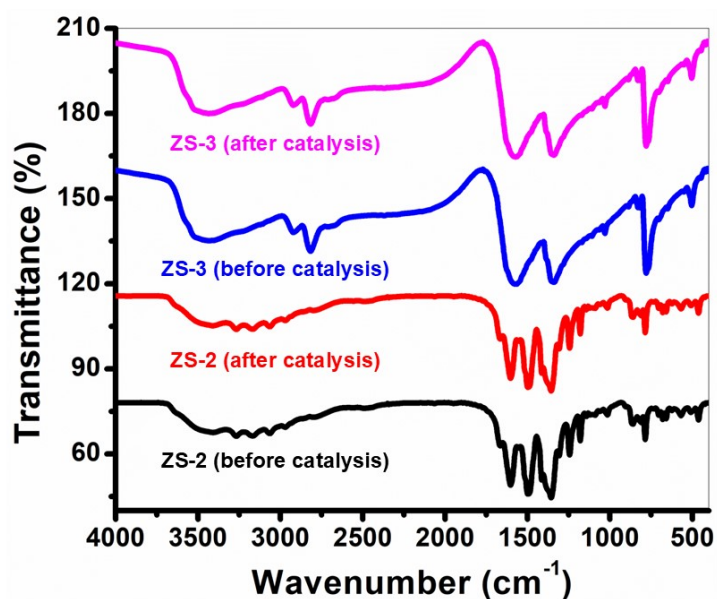


Fig. S18. FTIR spectra of ZS-2 and ZS-3 before and after catalysis.

Calculations involved in the catalytic conversion of CO₂

$$\text{Conversion (\%)} = \frac{\text{Moles of reacted epoxide}}{\text{Total moles of epoxide}} \times 100$$

$$\text{Selectivity (\%)} = \frac{\text{Moles of cyclic carbonate}}{\text{Moles of reacted epoxide}} \times 100$$

$$\text{Yield (\%)} = \frac{\text{Moles of cyclic carbonate formed}}{\text{Total moles of epoxide used}} \times 100$$

$$\text{TON} = \frac{\text{Moles of cyclic carbonate formed}}{\text{Moles of MOF catalyst used}}$$

$$\text{TOF} = \frac{\text{TON}}{\text{Reaction time (hrs)}}$$

References

- S1.** H. T. Chen, L. M. Fan, X. T. Zhang, L. F. Ma. Nanocage-Based InIII{TbIII}2 -Organic Framework Featuring LotusShaped Channels for Highly Efficient CO₂ Fixation and I₂ Capture. *ACS Appl. Mater. Interfaces*. **2020**, *12*, 27803-27811.
- S2.** B. Ugale, S. S. Dhankhar, C. M. Nagaraja, Exceptionally Stable and 20-Connected Lanthanide Metal–Organic Frameworks for Selective CO₂ Capture and Conversion at Atmospheric Pressure. *Cryst. Growth Des.* **2018**, *18*, 2432–2440.
- S3.** T. Zhang, H. T. Chen, S. R. Liu, H. X. Lv, X. T. Zhang, Q. L. Li, Highly Robust {Ln4}-Organic Frameworks (Ln = Ho, Yb) for Excellent Catalytic Performance on Cycloaddition Reaction of Epoxides with CO₂ and Knoevenagel Condensation. *ACS Catal.* **2021**, *11*, 14916–14925.
- S4.** L. Shang, X. L. Chen, L. Liu, M. Cai, R. K. Yan, H. L. Cui, H. Yang, J. J. Wang, Catalytic performance of MOFs containing trinuclear lanthanides clusters in the cycladdition reaction of CO₂ and epoxide. *J. CO₂ Util.* **2022**, *65*, 102235.
- S5.** N. Wei, R. X. Zuo, Y. Y. Zhang, Z. B. Han, X. J. Gu. Robust high-connected rare-earth MOFs as efficient heterogeneous catalysts for CO₂ conversion. *Chem. Commun.* **2017**, *53*, 3224- 3227.
- S6.** N. Wei, Y. Zhang, L. Liu, Z. B. Han, D. Q. Yuan. Pentanuclear Yb(III) cluster-based metal-organic frameworks as heterogeneous catalysts for CO₂ conversion. *Applied Catalysis B: Environmental*. **2017**, *219*, 603-610.

S7. Zalomaeva, O. V; Chibiryayev, A. M.; Kovalenko, K. A.; Kholdeeva, O. A.; Balzhinimaev, B. S.; Fedin, V. P. Cyclic Carbonates Synthesis from Epoxides and CO₂ over Metal–Organic Framework Cr-MIL-101. *J. Catal.* **2013**, *298*, 179–185.

S8. Chen, J.; Shen, K.; Li, Y. Greening the Processes of Metal–Organic Framework Synthesis and Their Use in Sustainable Catalysis. *ChemSusChem* **2017**, *10* (16), 3165–3187.

S9. Wang, S.; Yao, W.; Lin, J.; Ding, Z.; Wang, X. Cobalt Imidazolate Metal–Organic Frameworks Photosplit CO₂ under Mild Reaction Conditions. *Angew. Chemie* **2014**, *126* (4), 1052–1056.

S10. Nath, K.; Karan, C. K.; Biradha, K. Metal–Organic Frameworks and Metal–Organic Framework-Derived N-Doped Porous Carbon Materials as Heterogeneous Catalysts: Chemical Fixation of Carbon Dioxide under Mild Conditions and Electrochemical Hydrogen Evolution. *Cryst. Growth Des.* **2019**, *19* (11), 6672–6681.